Design and Optimization of A High Power Density Low Voltage DC-DC Converter for Electric Vehicles

Yang Chen, Wenbo Liu, Andrew Yurek, Xiang Zhou, Bo Sheng, Yan-Fei Liu, *Fellow, IEEE*

Department of Electrical and Computer Engineering, Queen's University, Kingston, ON, Canada

Email: yang.chen@queensu.ca, liu.wenbo@queensu.ca, 13aty@queensu.ca; xiang.zhou@queensu.ca; bo.sheng@queensu.ca, yanfei.liu@queensu.ca

***Abstract*— This paper presents a high power density LLC converter for Electric Vehicles (EVs) on-board low voltage DC-DC converter. The design specification imposes critical challenges on size and efficiency due to extremely high load current rating and wide input/output voltage range. The proposed design enables high switching frequency by using wide-band-gap (WBG) devices to significantly reduce the size of magnetic components and meet the power density requirement. A two-transformer configuration with series connected primary windings and parallel connected secondary windings is used to reduce the heavy I2R loss on the output side. The structures of parallel resonant inductor and transformers are carefully designed to reduce the fringing loss and AC conduction loss. A single phase 1.3kW LLC prototype with water cooling was built and experiment results verified the design considerations. The prototype achieved 3kW/L of power density and 97% peak efficiency. Full input voltage range from 250V to 430V and output voltage from 9V to 16V operation was verified with 96.5% efficiency achieved at nominal input and full load.**

Keywords*— *LLC, resonant converter, high power density, low voltage, wide voltage range, electric vehicles, EV, OBC, switch controlled capacitor, SCC.

I. Introduction

With the increasing demand of environmentally friendly energy, the research and development of electric vehicles (EV) technologies gains increased interest and significance. For an EV power system, a low voltage DC-DC converter (LDC) is required to convert the power from the high voltage (HV) battery (250V to 430V) to low voltage (LV) battery (9V to 16V). Fig. 1 shows the battery system of EVs. In general, HV batteries are used for traction of motor drives. LV batteries provides power to auxiliary equipment, such as lighting, audio, air conditioners, automatic seats etc. This way, the existing auxiliary equipment used for gas-powered vehicles can still be used in EVs. The required power for the LDC can be as high as kilowatts with the output current at hundreds of amperes, which is a big challenge from improving the efficiency and size point of view. Historically, studies and experiments are carried out based on phase-shift full bridge converter [1]-[5]. Current-doubler circuit and synchronized rectifier (SR) are also investigated to improve the heavy load efficiency [1]-[3].

LLC converter is widely used in datacenter and server applications at kilowatts level and has been proved to be

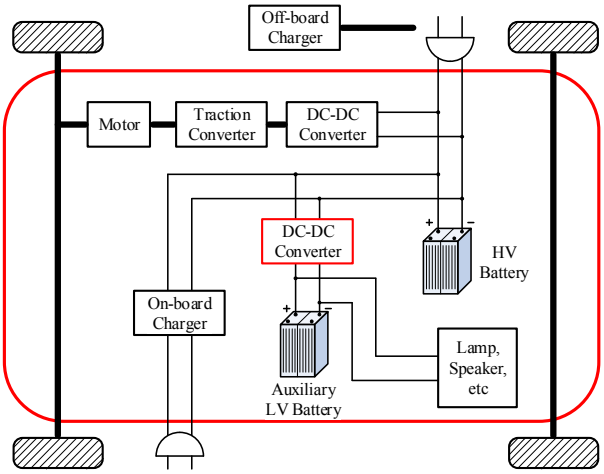

compact and efficient. Zero voltage switching (ZVS) on the primary side semiconductors and zero current switching (ZCS) on secondary side semiconductors can be easily achieved, thus switching noise and switching loss naturally maintain at very low level. Soft switching also allows LLC converter to switch at higher frequencies, which enables using of smaller magnetic components. Multi-phase interleaving technology can increase the current capacity and reduce the voltage ripple on the capacitor filter, allowing to use smaller capacitor filter. Besides, the switch-controlled capacitor (SCC) technology for LLC can achieve current sharing very efficiently and accurately [6]. So, a multiphase interleaved LLC converter with SCC would be a good candidate of the DC-DC converter used for EVs. Fig. 2 shows the configuration of a three phase SCC-LLC converter used as the LDC in the EV applications.

Since the benefits and operation of the SCC circuit have been extensively discussed in prior art [7]-[10], this paper will focus on the design of one phase of LLC converter instead of multiphase operation. The design challenge here is the heavy current stress, especially on the secondary side. To mitigate the impact of high current, full bridge is used on the primary side rather than a half bridge to reduce the primary current to half. Also, GaN HEMT with superior figure of merit is used with switching frequency of 500kHz. With this, the magnetics

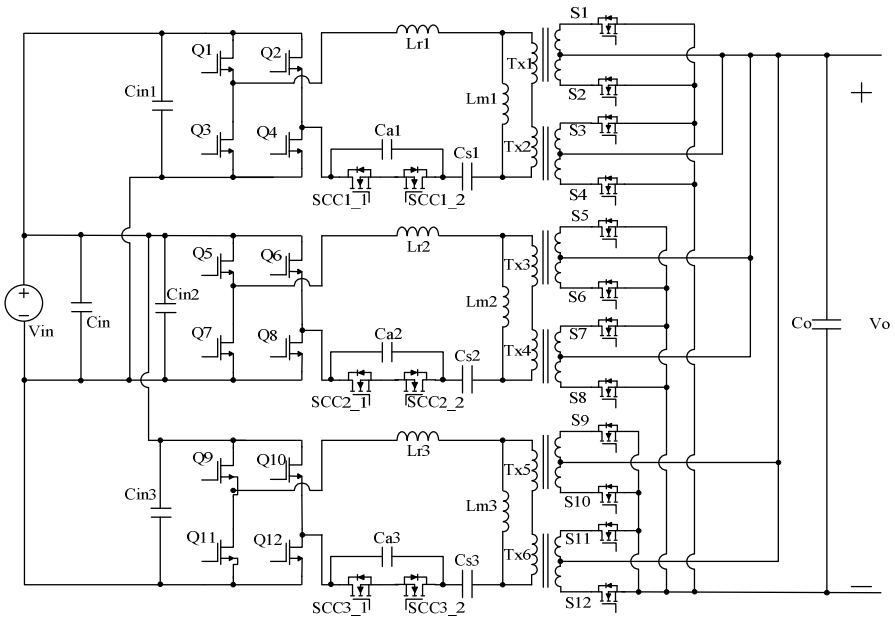

Fig. 2. Three-phase interleaved full wave SCC-LLC resonant converter

components size is expected to reduce a lot as compared to existing designs with a frequency of 100kHz range. For the 90A max current on the secondary side, two transformers are used to split the current even for each phase. The total conduction loss is reduced to half and becomes manageable within a PQ 35/35 core. Besides, the transformer is connected in a center-tapped manner to minimize the conduction loss of the synchronous rectifiers (SR). Multiple SRs are paralleled with optimized layout and cooling on PCB. Last not least, the magnetics are optimized to reduce the fringing loss on the inductor and the skin effect loss of the transformers.

The paper is organized as follows: Section II presents the design considerations of resonant parameters. Section III analyzes the problems of the magnetic components and discusses the loss reduction approach. Section IV performs a series of experimental results and Section V concludes the paper.

II. Selection of Resonant Component Parameters

Proper design of the magnetic components (L_r, L_p and transformer) is critical to maximize the power capacity within limited component size. Table. 1 shows the required specification of the design.

Conventionally, LLC converters operates in the below resonance region to maximize the performance. This means the converter operates as a step-up converter. The resonant point (voltage gain is unity) is selected based on the maximum input voltage and minimum output voltage. The transformer turns ratio is determined by (1), where N_p is the primary turns and N_s is the secondary turns number.

$$n = N_p : N_s = V_{in\_max} : V_{o\_min} \quad (1)$$

Table 1 Specifications of the LDC converter

Vin range:	250V to 430V
Vout range:	9V to 16V
Rated Vout:	14V
Switching Frequency	250kHz ~ 500kHz
Maximum Iout	270A for Vin > 330V
	160A for Vin < 330V
Maximum Pout	3,800W (14V at 270A)
Max efficiency	> 96%
Power density	3kW / Liter

With 430V max input and 9V min output voltage, each transformer turns ratio should be 430V / 9V / 2 = 23.8. However, as 9V is an odd point with less current requirement, final turns are selected as 22:1:1 for each transformer. This is selected based on the trade-off between gain requirement, nominal operation optimization and utilization of window areas of transformers.

In order to increase the power density, the switching frequency of the converter is designed to be 250kHz to 500kHz. The resonant inductor is selected as 25uH and the resonant capacitor is selected as 3.4nF based on known LLC design methods.

The selection of L_p is a tradeoff between the voltage gain (current capacity) and efficiency. A major barrier of high current LLC converter is that L_p value should be low enough to achieve required voltage gain. High circulation current will be induced when the L_p value is small and this it will increase the conduction loss on primary side. However, since the primary current is very low as compared to the secondary, and GaN switches are used with superior low Rdson and switch loss, the

overall efficiency is not significantly sacrificed with a small L_p to cover the full range of gain requirement.

In the studied case, load capacity is different at different input condition. For 320V to 430V, the converter is rated for full power, while for 250V to 320V input voltage, only 60% load current is required. This signifcantly alleviated the gain design burden. Finally, L_p is selected as 125uH.

III. Practical Measures to Improve the Performance of Single Phase LLC Converter

A. Structural Modification of High Power Magnetics

Magnetic components are the most critical design target in an LLC converter to achieve high efficiency. One challenge in the design is from the L_p. Conventionally, L_p is implemented by using the magnetizing inductor of the transformer. However, in this application, the L_p value is relatively small and a big air gap (even not applicable) on the transformer core is required to reduce the magnetizing inductor to the desired value. This can add a significant amount of fringing loss to the transformer winding, which already carries the massive current on the secondary side. In order to reduce the conduction loss, a separate L_p is used instead of the integrated. On one hand, it can avoid the extra fringing loss. On the other hand, it shunts the high circulation current so that transformer primary winding current is reduced.

In this design, to maintain the full input and output voltage range, the L_p inductance value is selected as relatively small. To achieve the optimal core and winding loss balance, 44 turns is selected with a 5mm air gap on a PQ35/35 core. The concern here is that the flux will go off rail on the edge of the air gap and enters far into the surrounded winding area. The high frequency fringing flux induces severe eddy current loss on the windings [7]. The fringing effect is more pronounced when the air gap is large. The power is determined in (2), where is μ_0 the permeability of the free space, ρ is the resistivity of conductor, H is fringing flux, f is the frequency, w is the width of the conductor, t is the thickness of the conductor.

$$P = \frac{1}{6\rho}(\pi \mu_0 H f)^2 w^3 \qquad (2) \quad (2)$$

ANSYS finite element analysis (FEA) model was built to simulate the eddy current loss around a large air gap. Fig. 3 illustrates the magnetic field of the studied case: several flux lines cut through the coil and loss is generated in the affected area.

To solve this problem, ideally a distributed air gap solution can mitigate the loss. However, it is difficult to implement in practice. In this paper, a two-section winding is used so that the copper wires are moved away from the air gap, as shown in Fig. 4. The windings width can be selected based on the density and effective area of the fringing flux.

The thermal images in Fig. 5 and Fig. 6 compare the impact induced by the fringing loss near the air gap. The converter is operated in nominal output voltage of 14V with no load current, thus the L_p current stress in same as full load while other components has minimal current stress. In other words, L_p generate the same amount of heat while the other components generated minimal heat. As shown in Fig. 5, the hot spot of winding is located near the airgap area. The winding temperature is 30 degree Celsius cooler on the two-section winding configuration. The measured loss of Lp is decreased by 3W by changing one coil winding into two separate windings and leaving no coil around the air gap. The light load efficiency is significantly improved.

One other considerable loss factor of the magnetic components is that the high current stress on the transformer

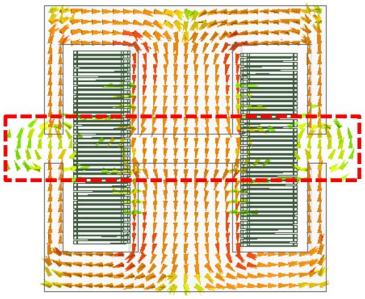

Fig. 3. Fringing flux cut through windings near air gap on traditional winding configuration

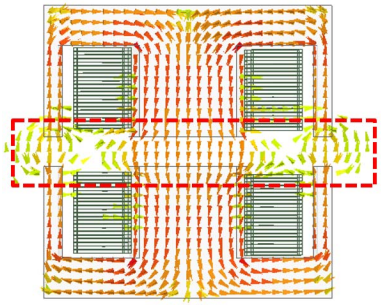

Fig. 4. Fringing flux on two-section winding configuration

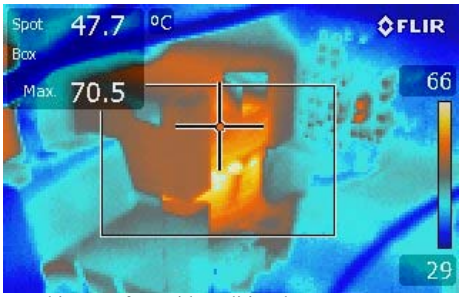

Fig. 5 Thermal image of Lp with traditional structure

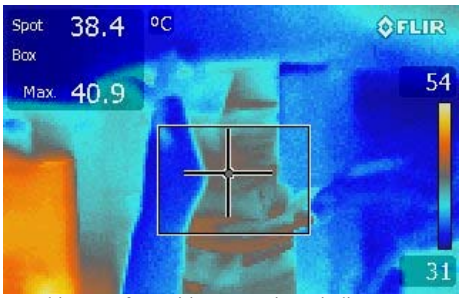

Fig. 6 Thermal image of Lp with two-section winding

secondary winding. With the high operating frequency of LLC converter, the skin dept δ is small and it introduce high AC resistance into the winding with thick foil. The skin depth δ is 0.12mm at 300kHz frequency, so a three-layer laminated 0.25mm copper foil is used instead of one 0.75mm single layer thick copper foil as the secondary winding.

B. Two-PCB Structure and Cooling System

Since the LDC will be used on EVs, where liquid cooling is already used for heat generating components such as electric motors and motor drives, the LDC can also benefit from the existing liquid cooling system to improve both performance and robustness.

The two-PCB structure is proposed as one PCB cannot fit all components of different heights space-efficiently. The objective is to improve the space utilization by separating magnetic components of larger height and ICs which are mounted on the PCBs' surface. Another consideration is that the control components should be separated from the power components because power components will need to attach to the cold plate of the liquid cooling system.

Fig. 7 shows the configuration of the two-PCB LDC converter of three phases. The upper PCB is the Control Board. All components related to control circuit are on the bottom side of the Control Board. The lower PCB is the Power Board. All components generating high heat (mostly primary and secondary semiconductors) are placed on the top side of the Power Board, where the bottom side is covered with large copper polygons and attached to the cold plate with thermal conducting insulation and copper bars. The heat generated by the semiconductors will be transferred to the cold plate through the extensive thermal vias between layers on the Power Board. The magnetic components are bolted to the top surface on the Control Board with no electrical connections. The leads are connected to the Power Board through power connectors. Such vertical configuration of PCBs greatly reduced the power loops and layout tradeoffs. It is also the critical design to achieve 3kW/L power density in this project.

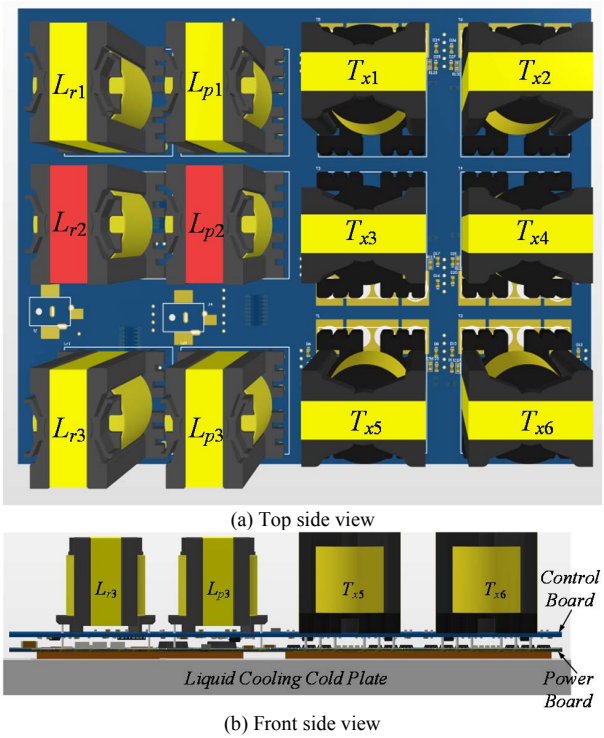

(a) Top side view

(b) Front side view

Fig. 7 3D model of the proposed two-PCB three-phase LLC converter

IV. Loss Analysis

In this section, the power loss of the main power circuit is analyzed. Particularly, conduction loss and turn-off loss of primary side switches, core loss and copper loss of magnetics, and conduction loss and gate driving loss of secondary side SRs are calculated.

A. Power Loss on Primary Side Switches

The simulation waveform at normal operation condition of 380V input, 14V/90A output is presented in Fig. 5.11. The switching frequency at the simulation point is 316kHz. The RMS current in *Lr* and *Lp* are 4.06A and 2.36A, respectively. Besides, the rms current of one secondary side SR is 44.75A. The peak current flowing through *Lr* and *Lp* are 6A and 3A, respectively.

Due to the ZVS operation, there is no turn-on loss for primary side devices. Taking advantage of low on-state resistance, GaN HEMT of GS66508B is used as the primary side switches. The key parameters of the GaN device are given in Table. 2.

Table. 2 Key parameters of GS66508B GaN HEMT

Primary device	250V to 430V
On-state resistance	50mΩ @ 6V, 25°C
	65mΩ @ 6V, 75°C
Output capacitance storage energy	8μJ
Switching energy during turn-off	7.5μJ

Considering the temperature rising in practice, the conduction loss of single GaN device is calculated as in (3).

$$P_{cond} = I_{rms}^2 R_{ds\_on} = \left(\frac{4.06}{\sqrt{2}}\right)^2 \times 65 = 535.7mW \qquad (3)$$

It is noted that the calculation of conduction loss does not include the dynamic resistor loss or the reverse conduction loss in the "body diode" of the GaN during deadtime.

The turn-off loss can be derived from the measured turn-off energy of the device in switching test minus the energy stored in the output capacitance from the datasheet. For each GaN device, the turn-off loss is derived as,

$$\begin{aligned} P_{turn-off} &= (E_{oss} - E_{off}) f_s \\ &= (8\mu J - 7.5\mu J) \times 316kHz \\ &= 158mW \end{aligned} \qquad (4)$$

B. Power Loss on Lr

Magnetic components are the most critical design target in an LLC converter to achieve high efficiency and high-power density. Since the designed converter mainly operates below 500kHz, 3C97 core material is selected, which is suitable for switching frequency lower than 500kHz.

PQ32/20 core is selected to for the resonant inductor Lr. The parameters of the PQ32/20 core are shown in Table 3. The maximum flux density at 380V input, 14V/90A output is derived as in (5).

Table. 3 Parameters of PQ 32/20 core

Core	PQ 32/20
Effective area	169 mm^2
Volume	9440 mm^3

$$B_{max} = \frac{L_r \times I_{Lr\_pk}}{N_{Lr} A_e} = \frac{25\mu H \times 6A}{15 \times 169mm^2} = 59.2mT \quad (5)$$

The core loss of the *Lr* can be estimated with Steinmetz equation as shown in (6),

$$P_{fe} = V_c K_c f^{\alpha} B^{\beta} = V_c P_c \quad (6)$$

Where, *Vc* is the core volume. Typical values of *Kc*, *α*, and *β* are given by the core material manufacturers. *Pc* is the core loss density. From the core material datasheet, the *Pc* value at 59.2mT Bmax and 70°C T is 0.095mW/mm3. Thus, the corresponding core loss of Lr is,

$$P_{fe} = V_c P_c = 9440mm^3 \times 0.095mW/mm^3 = 896.8mW \quad (7)$$

For LLC converters, the impact of high frequency effect on the winding cannot be ignored. Litz wire is used to minimizing the AC losses due to skin and proximity effect. The winding is realized using 15 turns of litz wire of NELC640/44SN with an outside diameter of 0.9mm. For Litz wire, the AC resistance factor for any number of strands can be derived as,

$$F_R = \frac{R_{ac}}{R_{dc}} = 1 + \frac{(\pi n N_s)^2 d_s^6}{192\delta^4 b^2} \quad (8)$$

Where, *n* is the number of strands used, *Ns* is the number of turns, *ds* is the strand diameter, *δ* is the skin depth, and *b* is the breath of the winding. All the parameters are given in Table 4.

Table. 4 Parameters of series resonant inductor winding

Number of strands	160
Strand diameter	0.0508 mm
Skin depth	0.13 mm
Breath of winding	8.9 mm

Substituting parameters of Table 4 into (8), the AC resistance factor *Fr* is calculated and equals to 5.16. Therefore, the copper loss of *Lr* can be derived as in (9), where *ILr_rms* is the rms current.

$$P_{cu} = I_{Lr\_rms}^2 \times R_{ac} = 4.06^2 \times 80.61m\Omega = 1.33W \quad (9)$$

C. Power Loss on Lp

PQ35/35 core with 3C97 material is used for L_p. Table 5 shows the core parameters. In addition, 44 turns of Litz wire of NELC1100/48SN with 1.5mm outside diameter is selected for the winding.

The maximum flux density of the L_p at the simulation condition is expressed as,

Table. 5 Parameters of PQ 35/35 core

Core	PQ 35/35
Effective area	190 mm^2
Volume	16300 mm^3

$$B_{max} = \frac{n \times V_{out}}{4 N_{Lm} A_e f_s} = \frac{44 \times 14V}{4 \times 44 \times 190mm^2 \times 316kHz} = 58.3mT \quad (10)$$

With 58.3mT B_{max} and 80°C T, the core loss can be derived as in (11),

$$P_{fe} = V_c P_c = 16300mm^3 \times 0.1 \frac{mW}{mm^3} = 1.63W \quad (11)$$

For LLC converters, the impact of high frequency effect on

$$B_{max} = \frac{L_r \times I_{Lr\_pk}}{N_{Lr} A_e} = \frac{25\mu H \times 6A}{15 \times 169mm^2} = 59.2mT \quad (12)$$

From (8), the AC resistance is calculated as 590mΩ. The corresponding copper loss is calculated as in (13),

$$P_{cu} = I_{Lm\_rms}^2 \times R_{ac} = 2.36^2 \times 590m\Omega = 3.29W \quad (13)$$

D. Power Loss on Tx

PQ35/35 core is also adopted to build the transformer. Considering the turns ratio of each transformer is 22, the primary side winding is achieved using 22 turns of litz wire of NELC640/44SN with an outside diameter of 0.9mm. Due to the massive output current, the secondary side winding is obtained by using three-layer paralleled 20mm × 0.25mm copper foil. The maximum flux density of each transformer can be calculated as,

$$B_{max} = \frac{n \times V_{out}}{4 N_{Lm} A_e f_s} = \frac{22 \times 14V}{4 \times 22 \times 190mm^2 \times 316kHz} = 58.3mT \quad (14)$$

where, N_{Tx} is primary side turns of the transformer. It should be noticed that the core loss of each transformer is same as the parallel resonant inductor because they are paralleled and has the same volt-sec as well as core size.

The copper loss of each transformer including primary side windings is derived as in (15) where the AC resistor is 68mΩ calculated from (8).

$$P_{cu} = I_{p\_rms}^2 \times R_{ac\_p} = \left(\frac{44.75 \times \sqrt{2}}{22}\right)^2 \times 68m\Omega = 0.56W \quad (15)$$

The copper loss of each transformer including primary side windings is derived as in (16) where the AC resistor is 2.51 mΩ calculated from (8).

$$P_{cu} = I_{s\_rms}^2 \times R_{ac\_s} = \left(44.75 \times \sqrt{2}\right)^2 \times 2.51m\Omega = 10.05W \quad (16)$$

The summary of the magnetics core loss and copper loss of single-phase LLC converter at 380V input, 14V/90A output is shown in Table 6.

Table. 6 Summary of magnetics core loss and copper loss

	Core loss	Copper loss
L_r	0.9 W	1.33 W
L_p	1.63 W	3.29W
T_{x1}	1.63 W	10.61 W
T_{x2}	1.63 W	10.61 W

E. Power Loss on Secondary Side SRs

Silicon MOSFET of TPHR8504PL is used as the secondary side SR. The Rdson is 1.25mΩ @ 5V, 75°C. In practice, three MOSFETs are connected in parallel to share output current. The total conduction loss of SRs connected to the two transformers can be calculated as in (17)

$$P_{cond} = I_{rms}^2 R_{ds\_on} = \left(44.75 \times \sqrt{2}\right)^2 \times \frac{1.25}{3} \times 2 = 3.34\ W \quad (17)$$

The Qg of the SR is 49nC @ 5V, thus the total driving loss for SRs of one phase is,

$$P_{drive} = Q_g V_{gs} f_s = 3 \times 49nC \times 5V \times 316kHz \times 4 = 0.93\ W \quad (18)$$

It should be noted that in practice the SRs can not conduct with 180-degree angle. In other words, the body diode will conduct for a short period of time during each switching cycle because the PCB trace inductance and package inductance tend to turn off the SR early, and this becomes significant with heavy current like in this case. Besides, the three paralleled SR might not be able to reduce the loss to one third in practice, because current tend to pick the shortest track and the actual current is not absolutely balanced in three SRs. Thus, the actual SR loss will be more than calculated.

V. Experiment Result

A three phase 3.8 kW prototype was built to verify the performances. Fig. 8 shows the setup. The LLC converter is assembled on a two-layer PCB with a dimension of 190mm*45mm, the total height is 49mm. A water-cooling system is installed to provide improved thermal performances, especially for the secondary side SRs with high current stress.

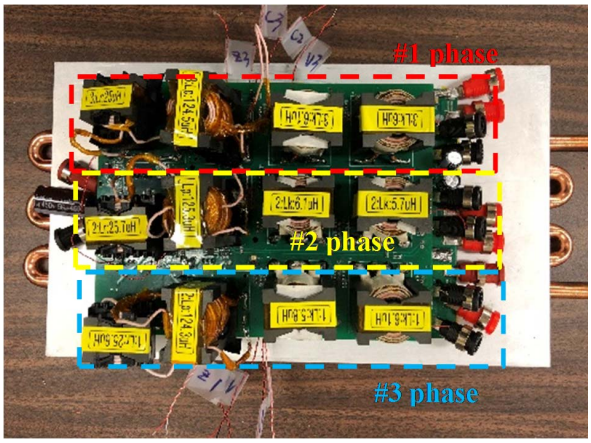

Fig. 8. Prototype of three-phase SCC-LLC LDC with liquid cooling

Table 7: Parameters and the designed three-phase LLC LDC

Transformer	N = 22:1:1, 2 in series on primary parallel on secondary PQ35/35 core
Parallel inductor	L_{m1} = 125.5μH, L_{m2} = 124.2μH, L_{m3} = 127.2μH, PQ35/35 core
Series inductor	L_{r1} = 26.1μH, L_{r2} = 25.7μH, L_{r3} = 26.1μH, PQ32/20 core
Series capacitor	C1808C681JGGAC7800 2KV, 680pF × 5 (per phase)
Primary side GaNs	GS66508B (650V, 30A) × 4 (per phase)
Secondary side SRs	TPHR8504PL (40V, 150A) × 12 (per phase)
SCC MOSFETs	IPB200N25N3 (250V, 64A) × 2 (per phase)
Output capacitor	C3216JB1E336M160AC, 25V, 33μF × 10 (per phase)
MCU	DSPIC33FJ32GS610 × 2

Table 7 shows the parameter designs and components selection the three phase LLC. And Table 8 shows the comparison of the proposed and existing solution.

Fig 9 shows the waveform of single-phase LLC converter at 430V input, 14V output with 20A and 90A output current. Before the GaN device is turned on, the corresponding drain to source voltage already drops to zero. Thus, ZVS is achieved for primary side GaN device.

Fig 10 shows the waveform at 380V input, 14V/90A output. The rms current flowing through series resonant inductor and parallel resonant inductor are 3.93A and 1.98A, which is close to the simulation results of 4.03A and 2.06A.

Fig. 11 illustrates the steady state waveform at 330V input, 14V/90A output. The switching frequency is 296kHz with peak current of 6.4A in the resonant tank. The measured RMS current is 4.15A.

Table 2 Comparison between Proposed and existing solution

Reference	*Input voltage*	*Output voltage*	*power*	*Peak efficiency*	*Full-load efficiency*	*Power density*	*Switching frequency*
[1]	200V~400V	12V	1.2kW	95.5%	90%	0.5kW/L	100kHz
[2]	235V~431V	11.5V~15V	2kW	93.5%	93%	0.94kW/L	200kHz
[3]	300V~400V	12V~16V	0.72kW	93.5%	90%	-	100kHz
[4]	220V~450V	6.5V~16V	2.5kW	93.2%	92%	1.17kW/L	90kHz~200kHz
[5]	200V~400V	12V	2kW	95.9%	94.2%	-	100kHz~133kHz
Proposed	250V~430V	9V~16V	1.3kW	96.7%	>96%	3.12kW/L	260kHz~400kHz

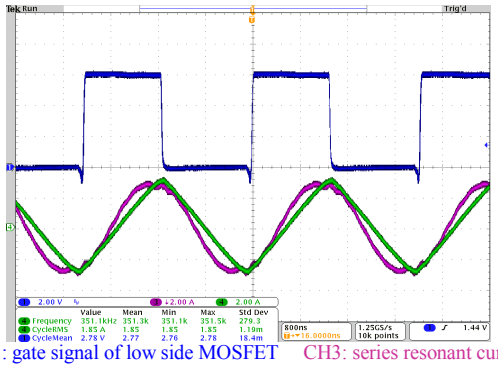

CH1: gate signal of low side MOSFET CH3: series resonant current
CH4: parallel resonant current
(a) 20A output current

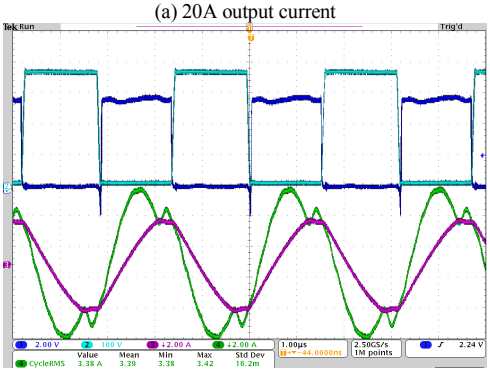

CH1: gate signal of low side GaN CH2: Vds of low side GaN
CH3: series resonant current CH4: parallel resonant current
(b) 90A output current

Fig. 9 Steady state waveform of single-phase LLC converter at 430V input, 14V/90A output

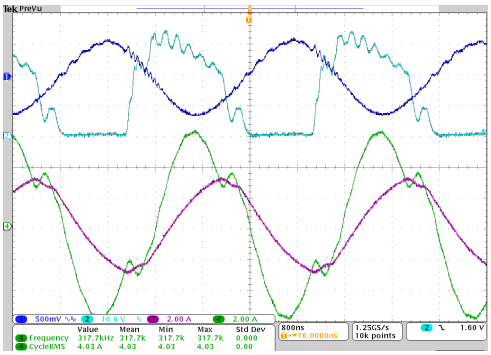

CH1: output voltage in AC coupling CH2: Vds of SR
CH3: series resonant current CH4: parallel resonant current

Fig. 10 Steady state waveform of single-phase LLC converter at 380V input, 14V/90A output

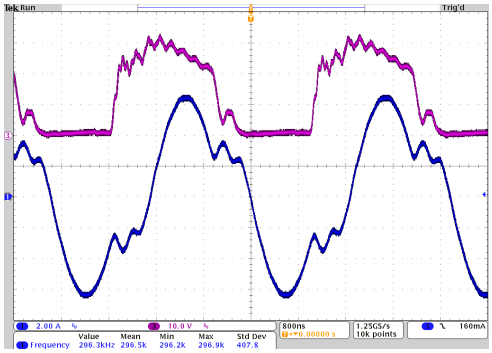

CH1: series resonant current **CH3: Vds of SR**

Fig. 11 Steady state waveform of single-phase LLC converter at 330V input, 14V/90A output

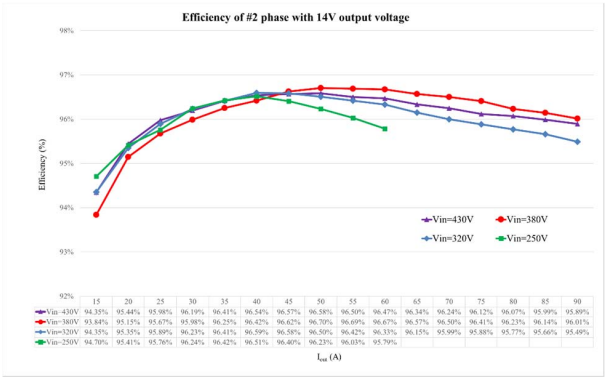

Fig. 12 Measured efficiency of the LLC at 14V Output and Different Vin

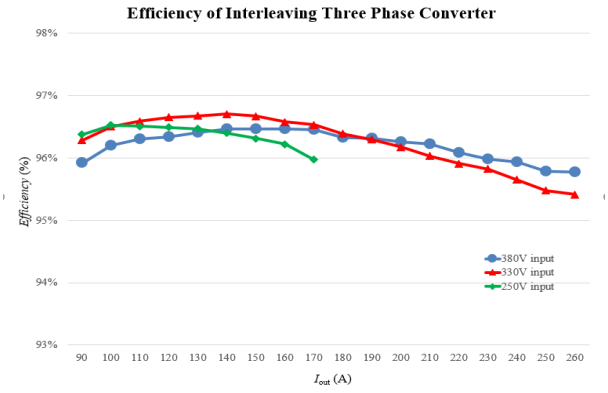

Fig. 13 Efficiency of three phase LLC at 14V Output and Different Vin

Fig. 12 shows the efficiency at 14V (target LV battery voltage) output and different input conditions. The peak efficiency of the converter is 96.7% at 55A load current with 380V-14V condition and the full load efficiency is above 96% for nominal input and above 95.5% for all other the cases. At 250V input, the total load requirement is derated to 60A.

The three phase LLC was operated with 60-degree interleaving. Fig. 13 shows the measured efficiency of three phase with total 260A load current. With such heavy load current, cooling becomes critical. The peak efficiency achieved is 96.7% with full load at 95.8%. The efficiency gap between this and the single phase could be caused by extra conduction loss due to components heated up.

VI. Conclusion

This paper presents the design considerations to optimize the performance in a three phase interleaved LLC converter for EVs. The three phase LLC take advantage of the SCC circuit to achieve highly balanced current sharing among phases. 3.12kW/L power density and more than 96% full load efficiency has been achieved. The proposed converter uses GaN HEMT and high switching frequency to significantly improve the power density. Two transformers are paralleled to carry the high load current and reduce the secondary I^2R loss. The parameters of resonant components are designed to cover the full input voltage range of 250V to 430V and output voltage from 9V to 16V. The large air gap fringing effect on L_p is much mitigated by separating the coil winding into two. The AC skin effect of the transformers is decreased by using three layer of laminated copper foils. Besides, the two-PCB configuration allows to make good use of the limited space as well as best utilize the liquid cooling.

References

[1] R. Hou and A. Emadi, "Applied integrated active filter auxiliary power module for electrified vehicles with single-phase onboard chargers," *IEEE Transactions on Power Electronics,* vol. 32, no. 3, pp. 1860-1871, Mar. 2017.

[2] D. Hamza, M. Pahlevaninezhad, and P. K. Jain, "Implementation of a novel digital active EMI technique in a DSP-based dc–dc digital controller used in electric vehicle (EV)," *IEEE Transactions on Power Electronics,* vol. 28, no. 7, pp. 3126-3137, Jul. 2013.

[3] R. Hou and A. Emadi, "A primary full-integrated active filter auxiliary power module in electrified vehicles with single-phase onboard chargers," *IEEE Transactions on Power Electronics,* vol. 32, no. 11, pp. 8393-8405, Nov. 2017.

[4] C. Duan, H. Bai, W. Guo and Z. Nie, "Design of a 2.5-kW 400/12V high-efficiency dc/dc converter using a novel synchronous rectification control for electric vehicles," *IEEE Transactions on Transportation Electrification,* vol. 1, no. 1, pp. 106-114, Jun. 2015.

[5] D. Moon, J. Park and S. Choi, "New interleaved current-fed resonant converter with significantly reduced high current side output filter for EV and HEV applications," *IEEE Transactions on Power Electronics,* vol. 30, no. 8, pp. 4264-4271, Aug. 2015.

[6] Z. Hu, Y. Qiu, Y. Liu, and P. C. Sen, "A Control Strategy and Design Method for Interleaved LLC Converters Operating at Variable Switching Frequency," *IEEE Transactions on Power Electronics,* vol. 29, no. 8, pp. 4426-4437, 2014.

[7] B. Sheng et al., "Adaptive Hysteresis Comparison Control of Load Sharing for Three-Phase Interleaved SCC-LLC Converter," 2020 *IEEE Applied Power Electronics Conference and Exposition (APEC),* New Orleans, LA, USA, 2020, pp. 3060-3067, doi: 10.1109/APEC39645.2020.9124377.

[8] X. Zhou et al., "A High Efficiency High Power-Density LLC DC-DC Converter for Electric Vehicles (EVs) On-Board Low Voltage DC-DC Converter (LDC) Application," 2020 IEEE Applied Power Electronics Conference and Exposition (APEC), New Orleans, LA, USA, 2020, pp. 1339-1346, doi: 10.1109/APEC39645.2020.9124278.

[9] X. Zhou et al., "Analysis and Design of SR Driver Circuit for LLC DC-DC Converter Under High Load Current Application," 2019 IEEE Energy Conversion Congress and Exposition (ECCE), Baltimore, MD, USA, 2019, pp. 1375-1381, doi: 10.1109/ECCE.2019.8912816.

[10] W. Liu, A. Yurek, Y. Chen, B. Sheng, X. Zhou and Y. Liu, "A High Power Density Thermal Management Approach Using Multi-PCB Distributed Cooling (MPDC) Structure," 2019 IEEE Energy Conversion Congress and Exposition (ECCE), Baltimore, MD, USA, 2019, pp. 4181-4188, doi: 10.1109/ECCE.2019.8912257.

[11] W. A. Roshen, "Fringing Field Formulas and Winding Loss Due to an Air Gap," in *IEEE Transactions on Magnetics*, vol. 43, no. 8, pp. 3387-3394, Aug. 2007.